Ultrabroadband Supercontinuum Generation and Frequency-Comb Stabilization Using On-Chip Waveguides with Both Cubic and Quadratic Nonlinearities

Daniel D. Hickstein, Hojoong Jung, David R. Carlson, Alex Lind, Ian Coddington, Kartik Srinivasan, Gabriel G. Ycas, Daniel C. Cole, Abijith Kowligy, Connor Fredrick, Stefan Droste, Erin S. Lamb, Nathan R. Newbury, Hong X. Tang, Scott A. Diddams, and Scott B. Papp

Phys. Rev. Applied **8**, 014025 — Published 24 July 2017

DOI: 10.1103/PhysRevApplied.8.014025

Ultrabroadband supercontinuum generation and frequency-comb stabilization using on-chip waveguides with both cubic and quadratic nonlinearities

Daniel D. Hickstein,[1,*] Hojoong Jung,[2] David R. Carlson,[1] Alex Lind,[1,3] Ian Coddington,[4] Kartik Srinivasan,[5] Gabriel G. Ycas,[1] Daniel C. Cole,[1,3] Abijith Kowligy,[1] Connor Fredrick,[1,3] Stefan Droste,[4] Erin S. Lamb,[1] Nathan R. Newbury,[4] Hong X. Tang,[2] Scott A. Diddams,[1,3] and Scott B. Papp[1]

[1] *Time and Frequency Division, National Institute of Standards and Technology, Boulder, Colorado 80305, U.S.A.*
[2] *Department of Electrical Engineering, Yale University, New Haven, Connecticut, 06520, U.S.A*
[3] *Department of Physics, University of Colorado, Boulder, Colorado, 80309, U.S.A.*
[4] *Applied Physics Division, National Institute of Standards and Technology, Boulder, Colorado 80305, U.S.A.*
[5] *Center for Nanoscale Science and Technology, National Institute of Standards and Technology, Gaithersburg, Maryland 20899, U.S.A.*
(Dated: June 19, 2017)

Using aluminum-nitride photonic-chip waveguides, we generate optical-frequency-comb supercontinuum spanning from 500 nm to 4000 nm with a 0.8 nJ seed pulse, and show that the spectrum can be tailored by changing the waveguide geometry. Since aluminum nitride exhibits both quadratic and cubic nonlinearities, the spectra feature simultaneous contributions from numerous nonlinear mechanisms: supercontinuum generation, difference-frequency generation, second-harmonic generation, and third-harmonic generation. As one application of integrating multiple nonlinear processes, we measure and stabilize the carrier-envelope-offset frequency of a laser comb by direct photodetection of the output light. Additionally, we generate ∼0.3 mW of broadband light in the 3000 nm and 4000 nm spectral region, which is potentially useful for molecular spectroscopy. The combination of broadband light generation from the visible through the mid-infrared, combined with simplified self-referencing, provides a path towards robust comb systems for spectroscopy and metrology in the field.

I. INTRODUCTION

Optical frequency combs are laser-based light sources that enable a wide variety of precision measurements, including the comparison of state-of-the-art atomic clocks [1], the quantitative measurement of pollution over several-kilometer paths above cities [2, 3], and even the search for distant Earth-like planets [4, 5]. Laser frequency combs are typically generated with relatively narrow (∼10 %) relative spectral bandwidth [6]. However, broad bandwidth is a requirement for many applications, such as spectroscopy, where it is desirable to probe several atomic or molecular transitions simultaneously, and optical frequency metrology, where stable lasers at different wavelengths must be compared. Consequently, narrowband frequency combs are usually spectrally broadened to at least one octave via supercontinuum generation (SCG) in materials with cubic nonlinearity ($\chi^{(3)}$), such as highly nonlinear fiber (HNLF) or photonic crystal fiber [7].

Moreover, octave-spanning bandwidth allows the carrier-envelope-offset frequency (f_{CEO}) of the frequency comb to be measured (and subsequently stabilized) using "f–2f" self referencing [8–10]. In the f–2f scheme, the low frequency portion of the spectrum undergoes second harmonic generation (SHG) in a material with quadratic nonlinearity ($\chi^{(2)}$), such as $LiNbO_3$, and interferes with the high-frequency portion of the spectrum, producing a signal that oscillates at f_{CEO}. Due to the modest effective nonlinearity of silica HNLF, SCG using traditional silica fiber requires high peak powers (typically 10 kW or more), which increases the electrical power requirements of the laser and limits the achievable repetition rates. Indeed, the adoption of new and compact frequency comb sources at gigahertz repetition rates, such as electro-optic combs [11, 12] and microresonator combs [6, 13, 14], is currently hindered by the difficulty of generating octave-spanning spectra using low-peak-power pulses. In addition, many potential applications of frequency combs require supercontinuum light at wavelengths that are difficult to achieve with SCG in silica fiber. In particular, light in the mid-infrared (3 µm to 8 µm) region is advantageous for molecular spectroscopy [15–19], but is absorbed by silica fiber.

Fortunately, on-chip photonic waveguides with wavelength-scale dimensions offer high confinement of light, which provides a substantial increase in the effective nonlinearity

$$\gamma = \frac{2\pi n_2}{\lambda A_{\mathrm{eff}}}, \tag{1}$$

where λ is the wavelength, A_{eff} is the effective area of the mode, and n_2 is the material-dependent nonlinear index, which is directly proportional to $\chi^{(3)}$ [7]. In addition, materials with higher $\chi^{(3)}$ – such as silicon nitride [20–27], silicon [28–30], aluminum gallium arsenide [31], and chalcogenide materials [32, 33] – further increase γ and allow much lower peak power (<1 kW) to be used for the SCG process. High confinement waveguides provide the additional advantage of increased control over the

* danhickstein@gmail.com

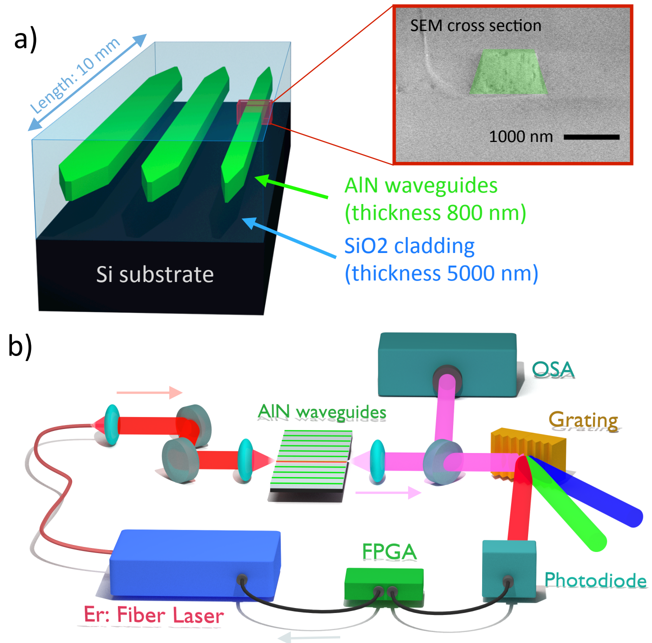

Figure 1. a) Aluminum nitride (AlN) on-chip waveguides embedded in SiO_2 tightly confine the light-field, providing high nonlinearity. b) To generate supercontinuum, 80-fs laser pulses (1560 nm, 800 pJ) are coupled into each waveguide. The broadband output is directed into an optical spectrum analyzer (OSA), or dispersed with a grating, where f_{CEO} is detected in the 780-nm region using a photodiode. The f_{CEO} signal is digitized using a field-programmable gate-array (FPGA), which applies feedback to the laser pump diode.

group-velocity dispersion (GVD), and therefore the spectral output of the SCG process.

Currently, supercontinuum generation in materials with both strong $\chi^{(2)}$ and $\chi^{(3)}$ nonlinearities is opening new possibilities for broadband light sources. For example, experiments with periodically poled $LiNbO_3$ (PPLN) have demonstrated supercontinuum generation via cascaded $\chi^{(2)}$ processes, and the simultaneous generation of supercontinuum and harmonic light [34–36]. Recently, aluminum nitride (AlN) has emerged as a lithographically compatible material that exhibits both strong $\chi^{(2)}$ and $\chi^{(3)}$ nonlinearities in addition to a broad transparency window. Consequently, thin-film AlN is proving to be a versatile platform for nanophotonics, providing phase-matched second-harmonic generation (SHG) [37], frequency comb generation [38], and ultraviolet light emission [39].

Here we present the first observations of SCG in lithographically fabricated, on-chip AlN waveguides and demonstrate that the platform provides exciting new capabilities: (1) We observe SCG from 500 nm to 4000 nm, and show the spectrum can be tailored simply by changing the geometry of the waveguide. (2) We find that the material birefringence induces a crossing of the transverse-electric (TE) and transverse-magnetic (TM) modes, which enhances the spectral brightness in a narrow band, and that the spectral location of this band can be adjusted by changing the waveguide dimensions. (3) We observe bright SHG, which is phase-matched via higher-order modes of the waveguide, as well as phase-mismatched difference frequency generation (DFG), which produces broadband light in the 3500 nm to 5500 nm region. (4) We demonstrate that simultaneous SCG and SHG processes in an AlN waveguide allows f_{CEO} to be extracted directly from the photodetected output, with no need for an external SHG crystal, recombination optics, or delay stage. (5) We use this simple scheme to lock the f_{CEO} of a compact laser frequency comb, and find that the stability of the locked f_{CEO} is comparable to a standard f–$2f$ interferometer and sufficient to support precision measurements.

II. EXPERIMENT

The fully SiO_2-clad AlN waveguides [38, 40] have a thickness (height) of 800 nm, and a width that varies from 400 nm to 5100 nm. Near the entrance and exit facets of the chip, the waveguide width tapers to 150 nm in order to expand the mode and improve the coupling efficiency, which is estimated at -4 dB/facet, on average. We generate supercontinuum by coupling into the waveguide approximately 80 mW of 1560 nm light from a compact, turn-key Er-fiber frequency comb [41], which produces ~80 fs pulses at 100 MHz. The polarization of the light is controlled using achromatic quarter- and half-waveplates. The light is coupled into each waveguide using an aspheric lens (NA=0.6) designed for 1550 nm. For output coupling, two different techniques are used, as shown in Fig. 1b. In the case of f_{CEO} detection, the light is out-coupled using a visible wavelength microscope objective (NA=0.85) and then dispersed with a grating before illuminating a photodiode. Alternatively, when recording the spectrum, the light is collected by butt-coupling a InF_3 multimode fiber (NA=0.26) at the exit facet of the chip. The waveguide output is then recorded using two optical spectrum analyzers (OSAs); a grating-based OSA is used to record the spectrum across the visible and near-infrared regions, while a Fourier-transform OSA extends the coverage to 5500 nm.

To model the supercontinuum generation, we perform numerical simulations using the nonlinear Schrödinger equation (NLSE), as implemented in the PyNLO package [42–45]. The effective refractive indices and effective nonlinearities of the waveguides are calculated using the vector finite-difference modesolver of Fallahkhair, Li, and Murphy [46]. The NLSE includes $\chi^{(3)}$ effects and incorporates the full wavelength dependence of the effective index, but it does not take into account any $\chi^{(2)}$ effects, higher order modes, or wavelength-dependent absorption.

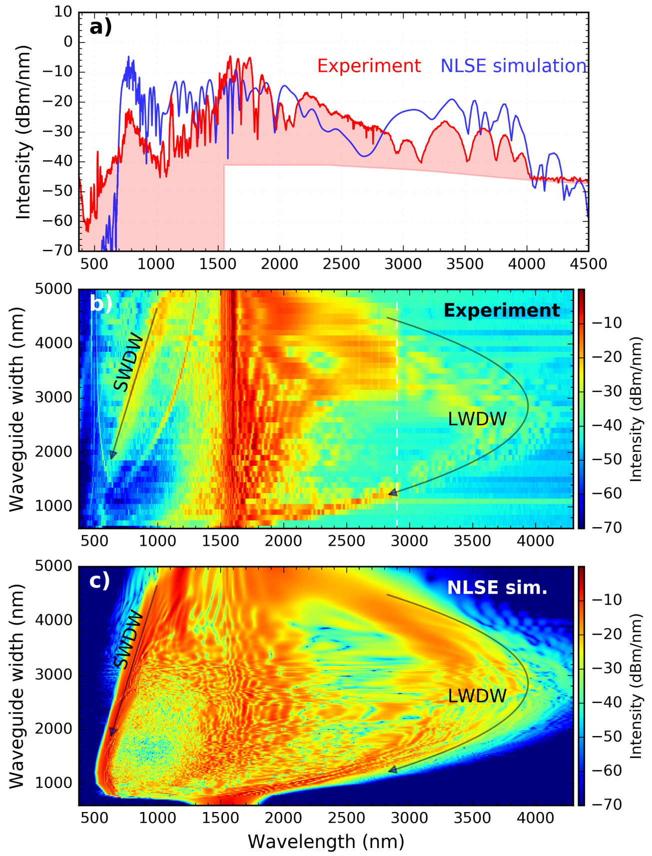

Figure 2. Supercontinuum generation from the lowest order quasi-transverse-electric (TE_{00}) mode. a) Experimental and theoretical optical spectrum from the 3200-nm wide waveguide (scaled by +7 dB to compensate for output-coupling to multimode fiber). The bottom of the shaded region indicates the noise-floor of the OSA. b) Experimentally observed spectra from all waveguide widths on the chip. The dashed line at 2900 nm indicates the onset of long-wavelength absorption in the waveguides. c) Simulated spectra using the Nonlinear Schrödinger Equation (NLSE) are in general agreement with experiment, and suggest that wavelength-dependent absorption is decreasing the amount of mid-infrared light observed experimentally. Solid lines indicate the short-wavelength and long-wavelength dispersive waves (SWDW and LWDW), and are in the same location in both (b) and (c).

III. RESULTS AND DISCUSSION

A. Supercontinuum from visible to mid-infrared

When pumped in the lowest-order quasi-transverse-electric mode (TE_{00}), the AlN waveguides generate light (Fig. 2) from the blue portion of the visible region (~500 nm) to the mid-infrared (~4000 nm). The broad peaks on both sides of the spectrum are the short-wavelength and long-wavelength dispersive waves (labeled "SWDW" and "LWDW" in Fig. 2b,c), which are generated at locations determined by the GVD of the waveguide [7, 47]. The broadband spectrum is a result of the flat GVD profile enabled by strong confinement of the light in these waveguides. The simulated spectra (Fig. 2c) reproduce the spectral location of thee long-wavelength and short-wavelength dispersive waves. However, the NLSE simulations overestimate the light intensity in the dispersive waves compared with the experiment. One reason for this discrepancy is that the waveguide mode at 1560 nm does not have perfect overlap with modes at different wavelengths, and the effective nonlinearity is actually smaller than what is predicted by Eq. 1, which assumes perfect mode-overlap. This effect is most pronounced at longer wavelengths, where the mode extends significantly outside of the waveguide and does not overlap well with the 1560 nm mode, which is mostly confined within the AlN waveguide.

When waveguide widths near 3500 nm are used, the supercontinuum shows high spectral intensity over a broad region from 1400 nm to 2800 nm, generally remaining within −20 dB of the transmitted pump intensity. This bright spectrum represents a promising source for molecular spectroscopy, since OH stretching transitions absorb in this region [48]. Indeed, sharp dips visible in the spectral intensity near 2700 nm are due to the absorption of water vapor in the OSA. Unfortunately, a sharp minimum in the spectrum near 2900 nm, and decreased intensity at wavelengths longer that 2900 nm suggests that these mid-infrared wavelengths are not efficiently transmitted through the waveguides. This loss is likely due to OH absorption [49] in the SiO_2, since a significant fraction of the mode extends outside the AlN waveguide and into the SiO_2 cladding at these wavelengths. In the future, the use of a different cladding material could increase the output of mid-infrared light. Nevertheless, the waveguides still produce usable, broadband light in the mid-infrared region – for example, we estimate that the 2600-nm waveguide produces ~0.3 mW in the 3500 nm to 4000 nm spectral region, which is sufficient power for some applications [50, 51]. Indeed, the mid-infrared light is easily seen in Fig. 2b, which presents spectra collected with just a few seconds integration time for each spectrum.

B. Brightness enhancement via a mode crossing

In the 800 nm to 1200 nm region, a sharp peak is seen in the supercontinuum spectrum for waveguide widths >1500 nm (Figs. 2b and 3c), which is not explained by the NLSE. The location of the peak occurs at the wavelength where the refractive index of the lowest order TE mode (TE_{00}) and a higher order quasi-TM mode (TM_{10}) cross (Fig. 3a). While such mode crossings are commonplace in Kerr-comb generation in microring resonators [52–54], they are not typically seen in supercontinuum generation in straight waveguides, because the TE_{00} usually has the highest effective index at all wavelengths. In the case of AlN waveguides, the polarization-mode crossing occurs because AlN is a birefringent material, and the bulk index for the vertical (TM) polarization is higher than for the horizontal (TE) polarization. At short wavelengths, where the waveguide geometry provides only a small modification to the refractive index, the TM modes tend to have the highest effective index. However, at longer wavelengths, geometric dispersion plays a larger role, lowering the effective index of the TM modes more than the TE modes and causing the polarization-mode crossing. Similarly, since modifications of the waveguide width tend to change the effective index of the TE modes more than the TM modes, the spectral location of the mode crossing also depends on the width of the waveguide (Fig. 3b).

A mode crossing causes a sharp feature in the GVD, which can allow for the phase-matching of four-wave-mixing processes in spectral regions that would otherwise be phase-mismatched [52, 53]. Indeed, the crossing of the TE_{00} and TM_{10} modes enables a strong enhancement of the supercontinuum spectrum in a spectral region that is otherwise dim. In some cases, this mode crossing enables a ∼25 dB enhancement of the spectral intensity. This enhancement enables a new degree of control over the spectral output, providing a narrow, bright region that could, for example, be used to measure a heterodyne beat with a narrow-band atomic-clock laser. It is not clear why the crossing with the TM_{10} mode is clearly seen in the experiment, while the crossings with the higher order TM modes are absent. Understanding what mechanism couples the modes, and how this coupling could be enhanced, would allow for further customization of the spectral output of this supercontinuum source.

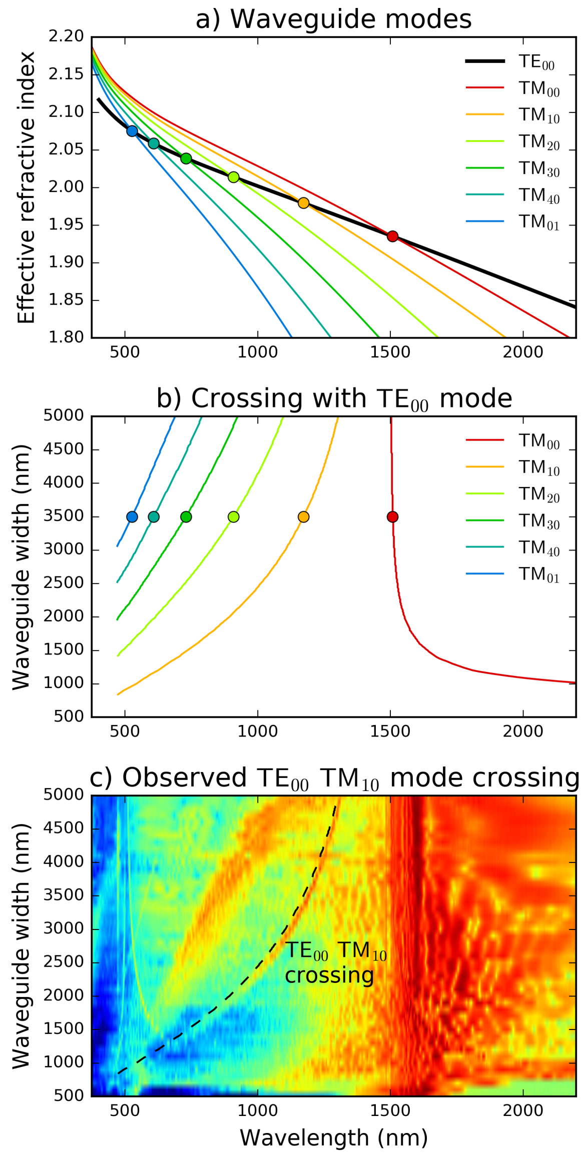

Figure 3. a) As the wavelength increases, the refractive index of the fundamental TE mode (TE_{00}) crosses several TM modes. A waveguide width of 3500 nm is shown. b) The spectral location of these polarization-mode crossings changes as a function of the waveguide width (shown) and thickness (not shown). c) The crossing of the TE_{00} and TM_{01} modes (as calculated from only the bulk refractive index and waveguide geometry) matches the location of the sharp peak in the experimental spectra.

C. Second harmonic generation and difference frequency generation

Since AlN has $\chi^{(2)}$ nonlinearity, it is capable of three-wave mixing processes, such as difference frequency generation (DFG), sum-frequency generation (SFG), and SHG. The thin AlN films used in this study are not single crystals, but instead consist of many hexagonal columns, which have the crystal z-axis oriented in the same (vertical) direction [40], but a random orientation for the other crystal axes. Consequently, while there is a strong $\chi^{(2)}$ component in the vertical (TM) direction, the $\chi^{(2)}$ in the horizontal (TE) direction is much weaker.

Indeed, we observe the strongest $\chi^{(2)}$ effects with the laser in the TM_{00} mode. The brightest SHG results from situations where the phase-velocity of the second harmonic in a higher order mode is the same as the phase velocity of the fundamental wavelength in the lowest order mode. This situation provides excellent phase matching, and we observe situations where the spectral intensity of the second harmonic light is on the same order-of-magnitude as that of the transmitted pump laser (Fig. 4a,b). However, this phase-matching mechanism provides a phase-matching bandwidth of only a few nanometers. Additionally, we also see third harmonic generation (THG), which is phase matched to higher order modes of the waveguide.

Under TM-pumping, the waveguides also produce broadband light in the 3500 nm to 5500 nm region via DFG (Fig. 4a,b). This process corresponds to the difference frequency between the spectrally broadened pump (1400 nm to 1700 nm) and the long-wavelength dispersive

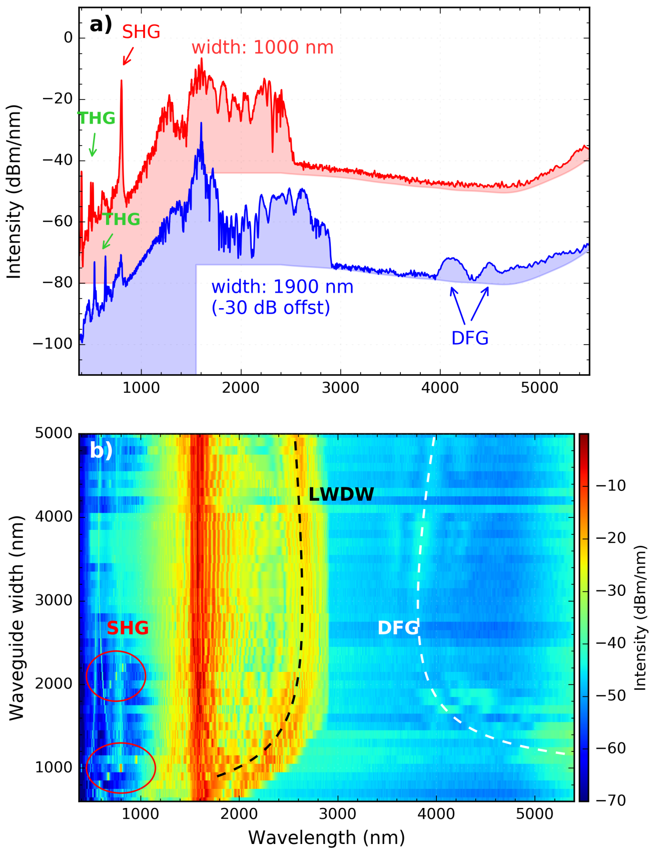

Figure 4. Supercontinuum generation from the lowest order quasi-transverse-magnetic (TM_{00}) mode. a) Experimental spectra from both the 1000-nm and 1700-nm width waveguides show simultaneous supercontinuum generation, second-harmonic generation (SHG), third-harmonic generation (THG), and difference-frequency generation (DFG). b) Experimental spectra from all waveguide widths, showing that waveguide geometry affects the positions of the long-wavelength dispersive wave (LWDW), the DFG peaks, and the phase-matched-SHG peaks.

wave (2000 nm to 2700 nm). As the waveguide width becomes narrower and the dispersive wave moves to shorter wavelengths, the DFG is pushed to longer wavelengths, as determined by conservation of (photon) energy. Indeed, for waveguide widths less than 1800 nm, the DFG moves to wavelengths longer than 5500 nm, which is outside of the range of our OSA. Additionally, the DFG process is strongly phase-mismatched, and therefore the conversion efficiency is low. However, in principle, it is possible to achieve phase matching by launching the pump laser into a higher-order mode of the waveguide.

D. f_{ceo} detection and comb stabilization

Since AlN exhibits both $\chi^{(2)}$ as well as strong $\chi^{(3)}$, f_{CEO} can be directly detected in the 780-nm region, as a result of simultaneous SHG and SCG. Unlike a traditional f–2f measurement, no interferometer is needed to set the temporal overlap of the interfering beams, and no additional alignment is necessary. The only equipment required to detect f_{CEO} is a 780-nm bandpass filter and a photodetector. Since these AlN waveguides have the strongest $\chi^{(2)}$ tensor component in the vertical direction, we observe the highest signal-to-noise ratio f_{CEO} signal when pumping in the TM_{00} mode. When TM pumping the 4800-nm-width waveguide, we achieve 37 dB SNR for the f_{CEO} peak (Fig. 5a). Interestingly, the highest SNR f_{CEO} was obtained from phase-mismatched SHG in the larger width waveguides, despite the fact that much higher efficiency phase-matched SHG was seen for waveguide widths near 1000 nm.

We speculate that the poor mode overlap between the supercontinuum (in the TM_{00} mode) and the phase-matched second harmonic (in a higher-order TM mode) hinders detection of the f_{CEO}. Indeed, a recent attempt to detect a f–$3f$ signal in SiN waveguides found that mode overlap severely limited the achievable SNR [55]. In contrast, the phase-mismatched SHG that takes place in the fundamental mode compensates for low conversion-efficiency with better overlap with the supercontinuum light. Furthermore, the highest SHG conversion likely takes place at the point of soliton fission, where the pulse is compressed and the peak intensity is the highest. This is the same point where most of the supercontinuum light is generated. Since the f and $2f$ signals are generated simultaneously, and propagate in the same waveguide mode, temporal overlap is provided automatically. Nevertheless, in future implementations, on-chip mode converters [56] could be used to provide both phase-matched SHG, as well as mode overlap, thereby providing higher f_{CEO} signal.

With the f_{CEO} detected directly from the waveguide output (Fig. 1b), we could achieve glitch-free f_{CEO} locking of a compact frequency comb for several hours (Fig. 5b). By recording the frequency of the f_{CEO} beat with an independent Π-type [57] frequency counter (Fig. 5c), we can verify that the f_{CEO} has been stabilized to a level comparable to what can be achieved with a traditional f–2f interferometer [41]. Unfortunately, thermal drifts in the input coupling prevented locking for more than a few hours without re-alignment. In the future, input and output coupling could be accomplished via fibers glued to the facets of the chip [58], which would effectively eliminate thermal drift in the coupling, and enable long-term stabilization of the laser comb.

IV. CONCLUSION

In summary, we have demonstrated aluminum nitride, a lithographically compatible material with strong $\chi^{(2)}$ and $\chi^{(3)}$ nonlinearities, as a promising material for on-chip supercontinuum generation and frequency comb self-referencing. Broadband light from 500 nm to 4000 nm

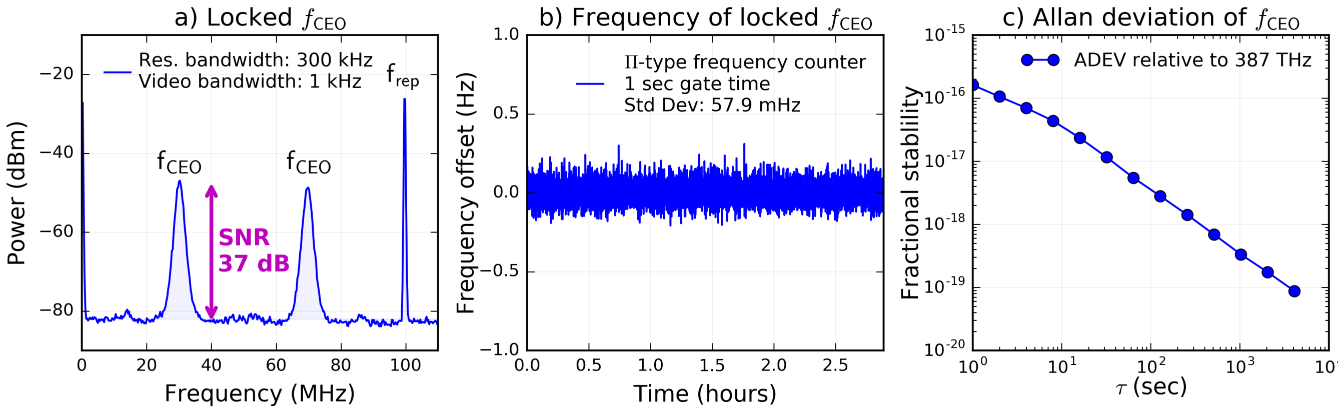

Figure 5. a) When the ∼780-nm region of the supercontinuum is detected with a photodiode, the $f_{\rm CEO}$ can be observed directly, without the need for an interferometer. b) The frequency of the locked $f_{\rm CEO}$ is stable over many hours. c) The (ordinary) Allan deviation of the frequencies shown in (b) demonstrates that the comb has been stabilized to a level suitable for precision metrology.

can be generated with only ∼80 mW (0.8 nJ) of 1560-nm pump power in the waveguide. Aluminum nitride provides an unexpected level of control over the output spectrum. In particular, the birefringence of the material enables a crossing of the TE and TM modes, which provides an enhancement in the spectral intensity by several orders of magnitude. In addition, we observe phase-mismatched difference frequency generation across the 3500 to 5500 nm region, which, if phase-matched, could provide a useful mid-infrared light source. Moreover, fully phase-matched second and third harmonic generation provide narrowband light that is tunable across the visible region.

Simultaneous second harmonic and supercontinuum generation processes allowed for the simplified detection of $f_{\rm CEO}$ using a single, monolithic waveguide, and enabled high-quality stabilization of a compact laser frequency comb. In conclusion, aluminum nitride waveguides provide both robust comb stabilization as well as access to broad spectra across the visible, near infrared, and mid-infrared regions. These capabilities are crucial ingredients for building inexpensive, portable frequency combs for field applications, such as dual comb spectroscopy, spectrograph calibration, and precision metrology.

ACKNOWLEDGMENTS

The authors thank Nima Nader, Jeff Chiles, Frank Quinlan, and Tara Fortier for helpful discussions, and acknowledge assistance in device fabrication provided by Yale cleanroom staff Michael Power and Michael Rooks.

This material is based upon work supported by the Air Force Office of Scientific Research under award number FA9550-16-1-0016, the Defense Advanced Research Projects Agency (DARPA) ACES, PULSE and SCOUT programs, the National Aeronautics and Space Administration (NASA), the National Institute of Standards and Technology (NIST), the National Research Council (NRC), and the National Science Foundation (NSF) Graduate Research Fellowship Program (GRFP).

[1] T. Rosenband, D. B. Hume, P. O. Schmidt, C. W. Chou, A. Brusch, L. Lorini, W. H. Oskay, R. E. Drullinger, T. M. Fortier, J. E. Stalnaker, S. A. Diddams, W. C. Swann, N. R. Newbury, W. M. Itano, D. J. Wineland, and J. C. Bergquist, "Frequency Ratio of Al^{+} and Hg^{+} Single-Ion Optical Clocks; Metrology at the 17th Decimal Place," Science **319**, 1808–1812 (2008).

[2] G. B. Rieker, F. R. Giorgetta, W. C. Swann, J. Kofler, A. M. Zolot, L. C. Sinclair, E. Baumann, C. Cromer, G. Petron, C. Sweeney, P. P. Tans, I. Coddington, and N. R. Newbury, "Frequency-comb-based remote sensing of greenhouse gases over kilometer air paths," Optica **1**, 290–298 (2014).

[3] E. M. Waxman, K. C. Cossel, G.-W. Truong, F. R. Giorgetta, W. C. Swann, S. Coburn, R. J. Wright, G. B. Rieker, I. Coddington, and N. R. Newbury, "Intercomparison of Open-Path Trace Gas Measurements with Two Dual Frequency Comb Spectrometers," Atmos. Meas.

Tech. Discuss. **2017**, 1–26 (2017).

[4] Chih-Hao Li, Andrew J. Benedick, Peter Fendel, Alexander G. Glenday, Franz X. Krtner, David F. Phillips, Dimitar Sasselov, Andrew Szentgyorgyi, and Ronald L. Walsworth, "A laser frequency comb that enables radial velocity measurements with a precision of 1 cm s^{-1}," Nature **452**, 610–612 (2008).

[5] Gabriel G. Ycas, Franklyn Quinlan, Scott A. Diddams, Steve Osterman, Suvrath Mahadevan, Stephen Redman, Ryan Terrien, Lawrence Ramsey, Chad F. Bender, Brandon Botzer, and Steinn Sigurdsson, "Demonstration of on-sky calibration of astronomical spectra using a 25 GHz near-IR laser frequency comb," Optics Express **20**, 6631–6643 (2012).

[6] T. J. Kippenberg, R. Holzwarth, and S. A. Diddams, "Microresonator-Based Optical Frequency Combs," Science **332**, 555–559 (2011).

[7] John M. Dudley, Gory Genty, and Stphane Coen, "Supercontinuum generation in photonic crystal fiber," Reviews of Modern Physics **78**, 1135–1184 (2006).

[8] David J. Jones, Scott A. Diddams, Jinendra K. Ranka, Andrew Stentz, Robert S. Windeler, John L. Hall, and Steven T. Cundiff, "Carrier-Envelope Phase Control of Femtosecond Mode-Locked Lasers and Direct Optical Frequency Synthesis," Science **288**, 635–639 (2000).

[9] R. Holzwarth, Th. Udem, T. W. Hnsch, J. C. Knight, W. J. Wadsworth, and P. St. J. Russell, "Optical Frequency Synthesizer for Precision Spectroscopy," Physical Review Letters **85**, 2264–2267 (2000).

[10] Scott A. Diddams, David J. Jones, Jun Ye, Steven T. Cundiff, John L. Hall, Jinendra K. Ranka, Robert S. Windeler, Ronald Holzwarth, Thomas Udem, and T. W. Hnsch, "Direct Link between Microwave and Optical Frequencies with a 300 THz Femtosecond Laser Comb," Physical Review Letters **84**, 5102–5105 (2000).

[11] T. Kobayashi, T Sueta, Y. Cho, and Y. Matsu, "High-repetitionrate optical pulse generator using a FabryPerot electrooptic modulator," Applied Physics Letters **21**, 341–343 (1972).

[12] Victor Torres-Company and Andrew M. Weiner, "Optical frequency comb technology for ultra-broadband radio-frequency photonics," Laser & Photonics Reviews **8**, 368–393 (2014).

[13] P. DelHaye, A. Schliesser, O. Arcizet, T. Wilken, R. Holzwarth, and T. J. Kippenberg, "Optical frequency comb generation from a monolithic microresonator," Nature **450**, 1214–1217 (2007).

[14] T. Herr, V. Brasch, J. D. Jost, C. Y. Wang, N. M. Kondratiev, M. L. Gorodetsky, and T. J. Kippenberg, "Temporal solitons in optical microresonators," Nature Photonics **8**, 145–152 (2014).

[15] Albert Schliesser, Nathalie Picque, and Theodor W. Hansch, "Mid-infrared frequency combs," Nature Photonics **6**, 440–449 (2012).

[16] Ian Coddington, Nathan Newbury, and William Swann, "Dual-comb spectroscopy," Optica **3**, 414–426 (2016).

[17] Gar-Wing Truong, Eleanor Waxman, Kevin C. Cossel, Fabrizio Giorgetta, William C. Swann, Ian R. Coddington, and Nathan R. Newbury, "Dual-comb Spectroscopy for City-scale Open Path Greenhouse Gas Monitoring," in *Conference on Lasers and Electro-Optics (2016), paper SW4H.2* (Optical Society of America, 2016) p. SW4H.2.

[18] Fabrizio R. Giorgetta, Gregory B. Rieker, Esther Baumann, William C. Swann, Laura C. Sinclair, Jon Kofler, Ian Coddington, and Nathan R. Newbury, "Broadband Phase Spectroscopy over Turbulent Air Paths," Physical Review Letters **115**, 103901 (2015).

[19] Kevin C. Cossel, Eleanor M. Waxman, Ian A. Finneran, Geoffrey A. Blake, Jun Ye, and Nathan R. Newbury, "Gas-phase broadband spectroscopy using active sources: progress, status, and applications [Invited]," JOSA B **34**, 104–129 (2017).

[20] Jorn P. Epping, Tim Hellwig, Marcel Hoekman, Richard Mateman, Arne Leinse, Ren G. Heideman, Albert van Rees, Peter J. M. van der Slot, Chris J. Lee, Carsten Fallnich, and Klaus-J. Boller, "On chip visible-to-infrared supercontinuum generation with more than 495 THz spectral bandwidth," Optics Express **23**, 19596–19604 (2015).

[21] Marco A. G. Porcel, Florian Schepers, Jrn P. Epping, Tim Hellwig, Marcel Hoekman, Ren G. Heideman, Peter J. M. van der Slot, Chris J. Lee, Robert Schmidt, Rudolf Bratschitsch, Carsten Fallnich, and Klaus-J. Boller, "Two-octave spanning supercontinuum generation in stoichiometric silicon nitride waveguides pumped at telecom wavelengths," Optics Express **25**, 1542–1554 (2017).

[22] Alexander Klenner, Aline S. Mayer, Adrea R. Johnson, Kevin Luke, Michael R. E. Lamont, Yoshitomo Okawachi, Michal Lipson, Alexander L. Gaeta, and Ursula Keller, "Gigahertz frequency comb offset stabilization based on supercontinuum generation in silicon nitride waveguides," Optics Express **24**, 11043–11053 (2016).

[23] A. S. Mayer, A. Klenner, A. R. Johnson, K. Luke, M. R. E. Lamont, Y. Okawachi, M. Lipson, A. L. Gaeta, and U. Keller, "Frequency comb offset detection using supercontinuum generation in silicon nitride waveguides," Optics Express **23**, 15440–15451 (2015).

[24] J. M. Chavez Boggio, D. Bodenmller, T. Fremberg, R. Haynes, M. M. Roth, R. Eisermann, M. Lisker, L. Zimmermann, and M. Bhm, "Dispersion engineered silicon nitride waveguides by geometrical and refractive-index optimization," JOSA B **31**, 2846–2857 (2014).

[25] Daniel Hickstein, Gabriel Ycas, Alex Lind, Daniel C. Cole, Katrik Srinivasan, Scott Diddams, and Scott Papp, "Photonic-chip Waveguides for Supercontinuum Generation with Picojoule Pulses," in *Advanced Photonics Conference* (Optical Society of America, 2016) p. IM3A.2.

[26] David Carlson, Daniel Hickstein, Alexander Lind, Judith Olson, Richard Fox, Roger Brown, Andrew Ludlow, Qing Li, Daron Westly, Holly Leopardi, Tara Fortier, Kartik Srinivasan, Scott Diddams, and Scott Papp, "Photonic-chip supercontinuum with tailored spectra for precision frequency metrology," arXiv:1702.03269 [physics] (2017).

[27] Adrea R. Johnson, Aline S. Mayer, Alexander Klenner, Kevin Luke, Erin S. Lamb, Michael R. E. Lamont, Chaitanya Joshi, Yoshitomo Okawachi, Frank W. Wise, Michal Lipson, Ursula Keller, and Alexander L. Gaeta, "Octave-spanning coherent supercontinuum generation in a silicon nitride waveguide," Optics Letters **40**, 5117–5120 (2015).

[28] Neetesh Singh, Darren D. Hudson, Yi Yu, Christian Grillet, Stuart D. Jackson, Alvaro Casas-Bedoya, Andrew Read, Petar Atanackovic, Steven G. Duvall, Stefano Palomba, Barry Luther-Davies, Stephen Madden, David J. Moss, and Benjamin J. Eggleton, "Midinfrared supercontinuum generation from 2 to 6 m in a silicon nanowire," Optica **2**, 797–802 (2015).

[29] I.-Wei Hsieh, Xiaogang Chen, Xiaoping Liu, Jerry I. Dadap, Nicolae C. Panoiu, Cheng-Yun Chou, Fengnian Xia, William M. Green, Yurii A. Vlasov, and Richard M. Osgood, "Supercontinuum generation in silicon photonic wires," Optics Express **15**, 15242–15249 (2007).

[30] Franois Leo, Simon-Pierre Gorza, Stphane Coen, Bart Kuyken, and Gunther Roelkens, "Coherent supercontinuum generation in a silicon photonic wire in the telecommunication wavelength range," Optics Letters **40**, 123–126 (2015).

[31] Minhao Pu, Hua Ji, Hao Hu, Luisa Ottaviano, Elizaveta Semenova, Pengyu Guan, Leif K. Oxenlwe, and Kresten Yvind, "Supercontinuum Generation in AlGaAs-On-Insulator Nano-Waveguide at Telecom Wavelengths," in *Conference on Lasers and Electro-Optics (2016), paper AM3J.3* (Optical Society of America, 2016) p. AM3J.3.

[32] Yi Yu, Xin Gai, Ting Wang, Pan Ma, Rongping Wang, Zhiyong Yang, Duk-Yong Choi, Steve Madden, and Barry Luther-Davies, "Mid-infrared supercontinuum generation in chalcogenides," Optical Materials Express **3**, 1075–1086 (2013).

[33] Michael R. E. Lamont, Barry Luther-Davies, Duk-Yong Choi, Steve Madden, and Benjamin J. Eggleton, "Supercontinuum generation in dispersion engineered highly nonlinear (gamma = 10 /W/m) As_2S_3 chalcogenide planar waveguide," Optics Express **16**, 14938–14944 (2008).

[34] Kana Iwakuni, Sho Okubo, Osamu Tadanaga, Hajime Inaba, Atsushi Onae, Feng-Lei Hong, and Hiroyuki Sasada, "Generation of a frequency comb spanning more than 3.6 octaves from ultraviolet to mid infrared," Optics Letters **41**, 3980–3983 (2016).

[35] Hairun Guo, Binbin Zhou, Michael Steinert, Frank Setzpfandt, Thomas Pertsch, Hung-ping Chung, Yen-Hung Chen, and Morten Bache, "Supercontinuum generation in quadratic nonlinear waveguides without quasi-phase matching," Optics Letters **40**, 629–632 (2015).

[36] Carsten Langrock, M. M. Fejer, I. Hartl, and Martin E. Fermann, "Generation of octave-spanning spectra inside reverse-proton-exchanged periodically poled lithium niobate waveguides," Optics Letters **32**, 2478–2480 (2007).

[37] Xiang Guo, Chang-Ling Zou, and Hong X. Tang, "Second-harmonic generation in aluminum nitride microrings with 2500%/W conversion efficiency," Optica **3**, 1126–1131 (2016).

[38] Hojoong Jung, Chi Xiong, King Y. Fong, Xufeng Zhang, and Hong X. Tang, "Optical frequency comb generation from aluminum nitride microring resonator," Optics Letters **38**, 2810–2813 (2013).

[39] S. Zhao, A. T. Connie, M. H. T. Dastjerdi, X. H. Kong, Q. Wang, M. Djavid, S. Sadaf, X. D. Liu, I. Shih, H. Guo, and Z. Mi, "Aluminum nitride nanowire light emitting diodes: Breaking the fundamental bottleneck of deep ultraviolet light sources," Scientific Reports **5**, 8332 (2015).

[40] Chi Xiong, Wolfram H. P. Pernice, and Hong X. Tang, "Low-Loss, Silicon Integrated, Aluminum Nitride Photonic Circuits and Their Use for Electro-Optic Signal Processing," Nano Letters **12**, 3562–3568 (2012).

[41] L. C. Sinclair, J.-D. Deschnes, L. Sonderhouse, W. C. Swann, I. H. Khader, E. Baumann, N. R. Newbury, and I. Coddington, "A compact optically coherent fiber frequency comb," Review of Scientific Instruments **86**, 081301 (2015).

[42] J. Hult, "A Fourth-Order Runge-Kutta in the Interaction Picture Method for Simulating Supercontinuum Generation in Optical Fibers," Journal of Lightwave Technology **25**, 3770–3775 (2007).

[43] A. M. Heidt, "Efficient Adaptive Step Size Method for the Simulation of Supercontinuum Generation in Optical Fibers," Journal of Lightwave Technology **27**, 3984–3991 (2009).

[44] Gabriel Ycas, Daniel Maser, and Daniel D. Hickstein, "pyNLO - Nonlinear optics modeling for Python," (2016).

[45] A. A. Amorim, M. V. Tognetti, P. Oliveira, J. L. Silva, L. M. Bernardo, F. X. Krtner, and H. M. Crespo, "Sub two cycle pulses by soliton self-compression in highly nonlinear photonic crystal fibers," Optics Letters **34**, 3851–3853 (2009).

[46] A. B. Fallahkhair, K. S. Li, and T. E. Murphy, "Vector Finite Difference Modesolver for Anisotropic Dielectric Waveguides," Journal of Lightwave Technology **26**, 1423–1431 (2008).

[47] Nail Akhmediev and Magnus Karlsson, "Cherenkov radiation emitted by solitons in optical fibers," Physical Review A **51**, 2602–2607 (1995).

[48] T. W. Graham Solomons and Craig B. Fryhle, *Organic Chemistry*, 10th ed. (Wiley, 2009).

[49] G. Navarra, I. Iliopoulos, V. Militello, S. G. Rotolo, and M. Leone, "OH related infrared absorption bands in oxide glasses," Journal of Non-Crystalline Solids **351**, 1796–1800 (2005).

[50] Daniel L. Maser, Gabriel Ycas, William I. Depetri, Flavio C. Cruz, and Scott A. Diddams, "Coherent frequency combs for spectroscopy across the 35 m region," Applied Physics B **123**, 142 (2017).

[51] Nima Nader, Daniel L. Maser, Daniel L. Maser, Flavio C. Cruz, Connor Fredrick, Connor Fredrick, Gabriel Ycas, Daron Westly, Richard Mirin, Jeffrey Shainline, Scott Diddams, and Scott Diddams, "Coherent on-chip spectral-engineered mid-IR frequency comb generation in Si waveguides," in *Conference on Lasers and Electro-Optics (2017), paper FTu3D.4* (Optical Society of America, 2017) p. FTu3D.4.

[52] Daniel C. Cole, Erin S. Lamb, Pascal Del'Haye, Scott A. Diddams, and Scott B. Papp, "Soliton crystals in Kerr resonators," arXiv:1610.00080 [physics] (2016), arXiv: 1610.00080.

[53] Sven Ramelow, Alessandro Farsi, Stphane Clemmen, Jacob S. Levy, Adrea R. Johnson, Yoshitomo Okawachi, Michael R. E. Lamont, Michal Lipson, and Alexander L. Gaeta, "Strong polarization mode coupling in microresonators," Optics Letters **39**, 5134–5137 (2014).

[54] T. Herr, V. Brasch, J. D. Jost, I. Mirgorodskiy, G. Lihachev, M. L. Gorodetsky, and T. J. Kippenberg, "Mode Spectrum and Temporal Soliton Formation in Optical Microresonators," Physical Review Letters **113**, 123901 (2014).

[55] David R. Carlson, Daniel D. Hickstein, Alex Lind, Stefan Droste, Daron Westly, Nima Nader, Ian Coddington, Nathan R. Newbury, Kartik Srinivasan, Scott A. Diddams, and Scott B. Papp, "Self-referenced frequency combs using high-efficiency silicon-nitride waveguides," Optics Letters **42**, 2314–2317 (2017).

[56] Xiang Guo, Chang-Ling Zou, Hojoong Jung, and Hong X. Tang, "On Chip Strong Coupling and Efficient Frequency Conversion between Telecom and Visible Optical Modes," Physical Review Letters **117**, 123902 (2016).

[57] S. T. Dawkins, J. J. McFerran, and A. N. Luiten, "Considerations on the measurement of the stability of oscillators with frequency counters," IEEE Transactions on Ultrasonics, Ferroelectrics, and Frequency Control **54**, 918–925 (2007).

[58] Hojoong Jung, Xiang Guo, Na Zhu, Scott B. Papp, Scott A. Diddams, and Hong X. Tang, "Phase-dependent interference between frequency doubled comb lines in a $\mathrm{X}^{(2)}$ phase-matched aluminum nitride microring," Optics Letters **41**, 3747–3750 (2016).